Calculation of Active Earth Pressure on the Retaining Wall with Limited-width Soil under a Curved Slip Failure Surface

Ziyu Tao, Xinxi Liu, Weiwei Wang

***Abstract*—Accurately calculating the active earth pressure of narrow backfill behind a retaining wall is crucial for safe construction and rational design. However, classical earth pressure theory cannot precisely forecast the nonlinear distribution of earth pressure behind a wall. This paper takes cohesionless soil behind a retaining wall as the research object to study the active earth pressure of narrow backfill behind a retaining wall—assuming that the failure surface consists of an integration of logarithmic spiral and straight lines—and takes into account the soil arching effect in the retaining wall translational mode. The expressions of the resultant active earth pressure and height of the resultant active earth-pressure application point are derived using the horizontal differential factor approach. The active earth-pressure calculation and experimental results of other methods were compared to verify the method validity, and the agreement was good, verifying the proposed method's rationality. The effects of such parameters as the soil–wall interface friction angle δ and backfill aspect ratio X_1/H on the active earth-pressure allocation and height of the resultant active earth-pressure application point are investigated using a parametric analysis. The outcomes reveal that the active earth-pressure value gradually grows as X_1/H increases, and the nonlinearity of the earth-pressure allocation curve becomes apparent. The height of the resultant active earth-pressure application point decreases gradually and is always greater than $H/3$, and $X_1/H = 0.5$ can be used as the critical ratio for finite and semi-infinite soils. As the soil–wall interface friction angle δ grows, the resultant active earth pressure declines significantly, and the height of the resultant active earth-pressure application point decreases gradually.**

***Index Terms*—Retaining wall, limited-width backfill, active earth pressure, principal stress trajectory, horizontal thin-layer element, curved slip failure surface**

I. Introduction

In urban slope projects, most new retaining walls are adjacent to existing basements or other underground structures and, hence, there is often only a narrow space available for backfill between the retaining wall and stable rock face. When the backfill width is narrow, its boundary conditions and damage mode do not conform to the classical earth pressure theory. Besides, the linear slip failure surface of the classical earth pressure theory does not match the actual curved slip failure surface. Thus, while both the Coulomb and Rankine earth pressure theories assume a linear allocation of the active earth pressure in the soil [1,2], numerous experimental results have indicated a nonlinear distribution because of the soil arching effect [3–5]. This objective effect is likely to occur because of lateral compression of the retaining wall when soil is confined behind it, thereby affecting the distribution and magnitude of the earth pressure. Therefore, the soil arching effect must be taken into account during the calculation of the active earth pressure in narrow backfill.

To this end, Handy [6] treated the shape of the soil arch between two parallel rough walls as a catenary-based plane, and got the earth-pressure allocation behind the wall after a rigorous mathematical derivation. Similarly, Harrop [7] found that soil arches in triangular sliding soil wedges constitute a catenary-based plane, and are very close to circular arcs when the minor and major principal stresses therein are assumed constant. Meanwhile, Paik [8] formed a novel formula for the active earth pressure of the retaining wall by assuming a circular trajectory for the minor principal stress, using the retaining wall surface and Rankine slip failure surface as the two end arches, while Goel [9] guessed a parabolic track for the minor principal stress.

Further, Xu [10] took into account the soil arching effect in the nonlimited state, used the upper limit of plasticity theory to obtain the failure surface angle and variation law for the lateral earth-pressure parameter by assuming various slip fracture surfaces, and derived an analytical expression of the active earth pressure of a narrow backfill. Meanwhile, Yu [11] proposed a novel approach to calculate the active earth-pressure of a rigid retaining wall by taking into account the effect of the intermediate principal stress and earth arching effect. Additionally, Dalvi and Pise [12] analyzed the approach to estimate the passive earth pressure by taking into account the shape of the failure surface and earth arch in the soil to be a catenary-based plane formed upward from the rough wall surface. Ying [13] took into account the horizontal differential factor method and the equations for the lateral earth pressure, thereby calculating the resultant active earth pressure and the height of its action point.

The basic premise of the above studies assumes that the soil failure surface is in the form of a straight line. However, the results of several model experiments have revealed that

Manuscript received January 6, 2022; revised May 31, 2022. The study was supported by the National Natural Science Foundation of China (NSFC Grants 51676041).

Yuzi Tao is an M.Sc. Student at the School of Civil Engineering, Changsha University of Science and Technology, Changsha 410114, China. (email: 1097806784@qq.com).

Xinxi Liu is a professor at the School of Civil Engineering, Changsha University of Science and Technology, Changsha, 410114, China. (email: liuxinxi1963@126.com).

Weiwei Wang is a lecturer at the School of Civil Engineering, Changsha University of Science and Technology, Changsha 410114, China. (corresponding author email: 12013032@hnist.edu.cn).

the slip failure surface of the limited-width soil behind the wall is either a logarithmic spiral line or an integration of a straight line and the arc of a logarithmic spiral [14–16]. For example, Chen [17] established a trapezoidal thrust model under a vertical rigid retaining wall constraint, and derived the governing equations for the soil pressure distribution and the resultant active earth pressure. In addition, He [18] tested the advection model of a retaining wall with various backfill width/height ratios of rigidity, and studied displacement and shear strain during active failure of the soil with the particle image velocimetry technique. Zhu [19] studied the failure characteristics of the passive earth pressure of sandy soil behind a flexible retaining wall with particle image velocimetry, thereby demonstrating a nonlinear drum-shaped distribution with increased lateral displacement. Meanwhile, Wang [20] used the variational equilibrium approach to estimate the active earth pressure by taking into account the shape of the logarithmic spiral slip failure surface in infinite soil. Furthermore, Yang [21] verified this assertion by experimenting on the failure of narrow backfill spaces behind rigid retaining walls under three different variational modes.

The above studies have demonstrated the validity of calculating the active earth pressure by using the curved–straight slip failure surface and taking into account the soil arching effect. Nevertheless, these two aspects must also be discussed separately for calculating the active earth-pressure allocation of limited-width soil more reasonably. Hence, the present paper takes into account the cohesionless soil behind the wall as the research object. In addition, expressions is derived with the limiting equilibrium method of the horizontal thin-layer element for the resultant active earth pressure of the cohesionless soil and the height of its point of application under narrow backfill conditions. The results are then compared with the previous literature conclusions in order to examine the influence of various backfill aspect ratios, wall–soil friction angles, and internal friction angles of the soil. The resulting analysis can provide a valuable reference for engineering design and application.

II. Basic Assumptions

For the convenience of the theoretical study in this paper, the following assumptions are made for the work.

1) It is assumed that the soil slip failure surface is a curved–straight slip failure surface by the wall heel.

2) The soil behind the wall is cohesionless soil with an internal friction angle of φ.

3) The back of the retaining wall is rough, and the friction angle between the retaining wall and soil is the same as that between the soil and existing building; both are δ.

4) The filing surface is horizontal, and there is no overload.

III. The Proposed Analytical Model

As illustrated in Fig. 1, the width and height of the limited soil are X_1 and H, respectively. The narrow backfill spaces behind the wall are divided into two separate zones, labelled Zone 1 and Zone 2, with heights of h_1 and h_2, respectively, and a horizontal differential element of height, dy, is considered in each Zone.

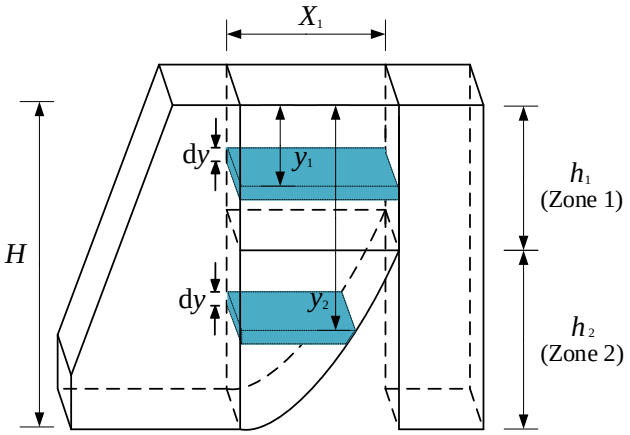

Fig. 1. A schematic diagram of the limited soil slip failure surface of the retaining wall.

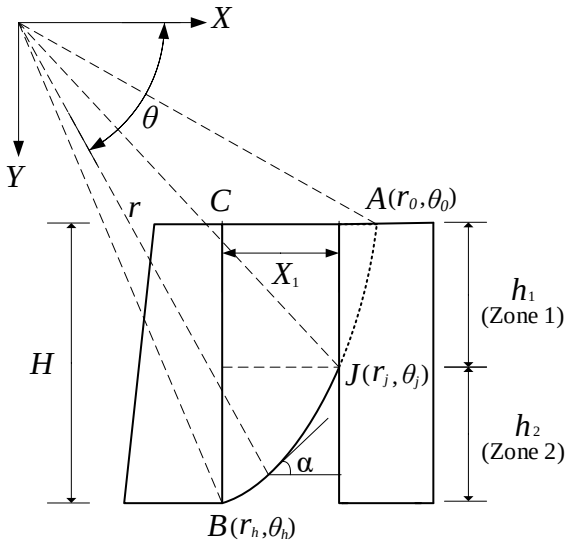

Fig. 2. A schematic diagram of the slip failure surface in the polar coordinate system.

With reference to Fig. 2, the logarithmic spiral line equation in the slip failure surface is derived by the variational equilibrium method [21] as follows:

$$r(\theta) = r_0 \exp\left(\theta - \theta_0\right)\tan\varphi \tag{1}$$

The rectangular coordinates of the backfill slip surface equation behind the wall are then expressed as follows:

$$\begin{cases} x = r_0 \exp\left[\left(\theta - \theta_0\right)\tan\varphi\right]\cos\theta \\ y = r_0 \exp\left[\left(\theta - \theta_0\right)\tan\varphi\right]\sin\theta \end{cases} \tag{2}$$

where r_0 is obtained from the geometric relationship in Fig. 2, as:

$$r_0 = \frac{H}{\exp\left[(\theta_h - \theta_0)\tan\varphi\right]\sin\theta_h - \sin\theta_0} \tag{3}$$

where θ_h is the polar diameter of point B in the coordinate system, and θ_0 is an arbitrary reference angle.

The slope of any point on the logarithmic spiral line is defined as k, and the angle of tangency is α; hence:

$$k = \tan\alpha = \frac{\mathrm{d}y}{\mathrm{d}x} = \tan\left(\frac{\pi}{2} + \varphi - \theta\right) \tag{4}$$

which leads to

$$\theta = \frac{\pi}{2} + \varphi - \alpha \tag{5}$$

The geometric relationship in Fig. 2 allows us to deduce the magnitude of θ_j:

$$r_j \cos\theta_j = r_h \cos\theta_h + X_1 \tag{6}$$

where θ_j is the polar diameter of point J in the coordinate system.

The theoretical derivation [12] and experimental phenomena [13] indicate that the soil failure surface is always located inside the Coulomb failure surface. The failure surface angle ψ, i.e., the angle between the horizontal line and the tangent line of the failure surface at the heel of the wall, is always larger than the Coulomb shear failure angle. Hence, it is sensible to consider the active earth pressure obtained when the failure surface angle is $\psi = \pi/4 + \varphi/2$. When $\theta = \theta_h$, ψ is equal to the logarithmic spiral line tangent angle α when crossing the wall heel. Substituting this information into Eq. (5) gives Eq. (7):

$$\theta_h = \frac{\pi}{2} + \varphi - \psi = \frac{\pi}{4} + \frac{\varphi}{2} \tag{7}$$

When θ_h is determined, the value of θ_0 can be arbitrarily chosen and substituted into Eq. (6) to find the corresponding θ_j. The heights of Zones 1 and 2 can then be derived using θ_j:

$$\begin{cases} h_1 = r_0 \exp[(\theta_j - \theta_0)\tan\varphi]\sin\theta_j - r_0 \sin\theta_0 \\ h_2 = H - h_1 \end{cases} \tag{8}$$

IV. Analysis of the Active Earth Pressure

A. The Equation for the Active Earth Pressure in Zone 1

When the back of the wall is displaced away from the soil direction, the friction between the wall and soil, and that between the deformed and stable soil, cause a deflection in the principal stress and form the minor principal stress arc trajectory. For calculation, the soil pressure in Zone 1 can be modelled as a rectangular area, as shown in Fig. 3.

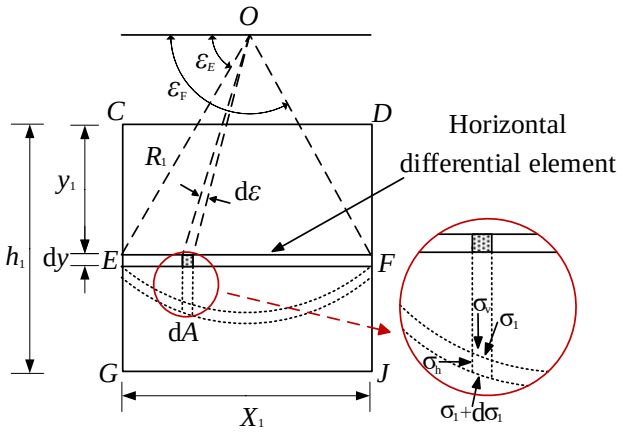

Fig. 3. A schematic diagram of the soil arch in Zone 1.

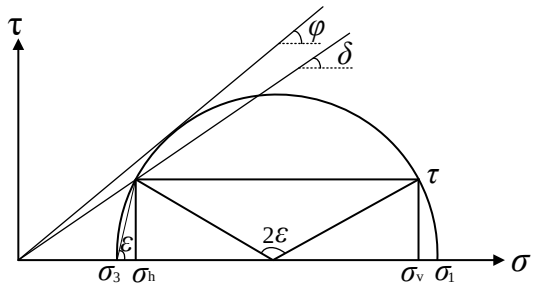

Fig. 4. Mohr's stress circle at Point E during active damage.

By removing point E from the horizontal differential layer of Fig. 3, the Mohr's stress circle of this point at active failure is revealed in Fig. 4. The vertical and horizontal stresses in Zone 1 are then expressed by Eq. (9):

$$\begin{cases} \sigma_{h1} = \sigma_1 \cos^2\varepsilon_E + \sigma_3 \sin^2\varepsilon_E \\ \sigma_{v1} = \sigma_1 \sin^2\varepsilon_E + \sigma_3 \cos^2\varepsilon_E \end{cases} \tag{9}$$

where ε_E means the angle between the horizontal direction and the major principal stress at point E.

Rankine's coefficient of lateral active earth pressure K_a is given by Eq. (10):

$$K_a = \sigma_3 / \sigma_1 = (1-\sin\varphi)/(1+\sin\varphi) \tag{10}$$

and the vertical force dV at point E is given by Eq. (11):

$$\mathrm{d}V = \sigma_{v1}\mathrm{d}A = \frac{\sigma_1[1-\cos(2\varepsilon)\sin\varphi]}{1+\sin\varphi} R_1 \sin\varepsilon \mathrm{d}\varepsilon \tag{11}$$

The relationship between the minor principal stress radius R_1 and the distance X_1 between points E and F is given by Eq. (12):

$$R_1 = \frac{X_1}{\cos\varepsilon_E - \cos\varepsilon_F} \tag{12}$$

Using the horizontal differential factor approach, the coefficient of lateral active earth pressure K_{awn1} in Zone 1 is given by the ratio of σ_{h1} to σ_{v1}, which can be derived as follows:

$$K_{awn1} = \frac{\sigma_{h1}}{\sigma_{v1}} = \frac{\cos^2\varepsilon_E + K_a \sin^2\varepsilon_F}{1 + \dfrac{(\cos^3\varepsilon_E - \cos^3\varepsilon_F)(K_a - 1)}{3(\cos\varepsilon_E - \cos\varepsilon_F)}} \tag{13}$$

where

$$\begin{cases} \varepsilon_E = \dfrac{\pi}{2} - \left[\arcsin\left(\dfrac{\sin\delta_1}{\sin\varphi}\right) - \delta_1\right] \Big/ 2 \\ \varepsilon_F = \dfrac{\pi}{2} + \left[\arcsin\left(\dfrac{\sin\delta_1}{\sin\varphi}\right) - \delta_1\right] \Big/ 2 \end{cases}$$

According to Fig. 5, a horizontal differential factor of width dy is taken at a distance y_1 from the surface of the narrow backfill. It is assumed that σ_{n1} is the lateral stress on the existing basement, τ_s and τ_w are the tangential stresses on the existing basement and the retaining wall, the self-weight of the horizontal differential factor is dw, and its length is the narrow backfill width X_1. Thus, the forces exerted on the horizontal differential element in Zone 1 are given by Eq.(14):

$$\begin{cases} \tau_{w1} = \sigma_{h1} \tan\delta \\ \tau_{s1} = \sigma_{h1} \tan\delta \\ dw_1 = \gamma X_1 dy \end{cases} \tag{14}$$

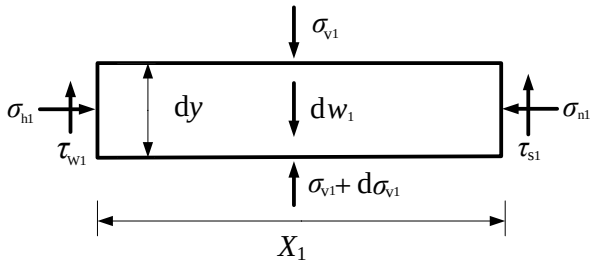

Fig. 5. The differential element model of Zone 1.

As the differential elements of force are balanced in the horizontal and vertical directions, their equilibrium can be inferred as follows:

$$\begin{cases} \sigma_{h1} dy = \sigma_{n1} dy \\ \sigma_{v1} X_1 + dw = (\sigma_{v1} + d\sigma_{v1}) X_1 + \tau_{s1} dy + \tau_{w1} dy \end{cases} \tag{15}$$

Substituting Eqns. (14) into Eq. (15) yields Eq. (16):

$$\frac{d\sigma_v}{dy} = \gamma - \frac{2\sigma_h \tan\delta}{X_1} = \gamma - \frac{2K_{awn1} \cdot \sigma_v \tan\delta}{X_1} \tag{16}$$

The horizontal earth pressure σ_{h1} is then given by Eq. (17):

$$\sigma_{h1} = Kawn_1 \cdot \sigma_{v1} \tag{17}$$

Finally, the resultant active earth pressure E_{a1} in Zone 1 is given by Eq. (18):

$$E_{a1} = \frac{\int_{A_2}^{A_1} \sigma_h dy}{\cos\delta} \tag{18}$$

where

$$A_1 = r_0 \sin\theta_0$$

$$A_2 = r_j \sin\theta_j = r_0 \exp[(\theta_j - \theta)\tan\varphi]\sin\theta_j$$

B. The Equation for the Active Earth Pressure in Zone 2

The soil pressure analysis model in Zone 2 includes the logarithmic spiral failure surface, as shown in Fig. 6.

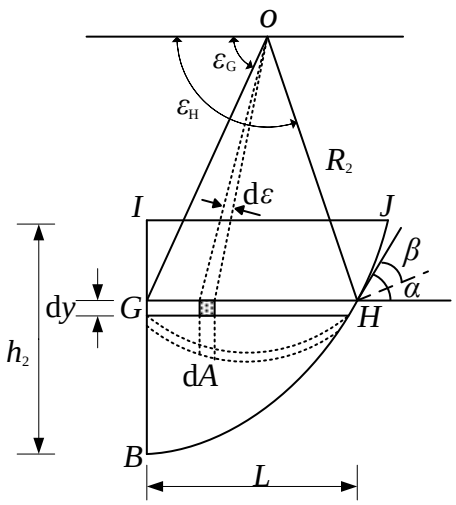

Fig. 6. A schematic diagram of the soil arch in Zone 2.

The vertical force *dV* applied to any point on the minor principal stress trajectory is given by Eq. (19):

$$dV = \sigma_v dA = \frac{\sigma_1 [1 - \cos(2\varepsilon)\sin\varphi]}{1 + \sin\varphi} R_2 \sin\varepsilon d\varepsilon \tag{19}$$

The association between the radius R_2 of the minor principal stress trajectory and the length L of the horizontal differential layer is given by Eq. (20):

$$R_2 = \frac{L}{\cos\varepsilon_G - \cos\varepsilon_H} \tag{20}$$

where

$$L = r_0 \exp[(\theta - \theta_0)]\cos\theta - r_h \cos\theta_h \tag{21}$$

The angle at point *G* can be obtained from Eq. (22):

$$\varepsilon_G = \pi/2 - \alpha_G/2 \tag{22}$$

where

$$\alpha_G = \left[\arcsin\frac{\sin\delta}{\sin\varphi} - \delta\right] \Big/ 2$$

On the failure surface, the limiting equilibrium condition indicates that the angle between the major principal stress and the tangent line of the failure angle at point *H* is $\beta = \pi/4 + \varphi/2$. Therefore, from the geometric relationship in Fig. 6, Eq. (23) is obtained:

$$\varepsilon_H = \pi/2 + \alpha - \beta = 3\pi/4 + \varphi/2 - \theta \tag{23}$$

The coefficient of the lateral active earth pressure K_{awn2} in Zone 2 can then be obtained as follows:

$$K_{awn2} = \frac{\sigma_{h2}}{\sigma_{v2}} = \frac{\cos^2\varepsilon_G + K_a \sin^2\varepsilon_H}{1 + \dfrac{(\cos^3\varepsilon_G - \cos^3\varepsilon_H)(K_a - 1)}{3(\cos\varepsilon_G - \cos\varepsilon_H)}} \tag{24}$$

where σ_{v2} and σ_{h2} are the vertical and horizontal stresses, respectively, in the horizontal differential factor of Zone 2.

A horizontal differential element of width d*y* is taken at distance y_2 from the soil surface, and α is the angle of tangency.

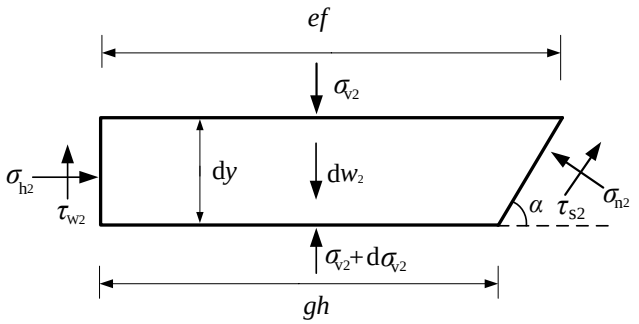

Fig. 7. The differential element model of Zone 2.

The lengths of the line segments of the horizontal differential element are as follows:

$$\begin{cases} ef = r\cos\theta - r_h \cos\theta_h \\ gh = ef - dy\tan(\theta - \varphi) \end{cases} \tag{25}$$

and the forces exerted on the horizontal differential element in Zone 2 are as follows:

$$\begin{cases} \tau_{w2} = \sigma_{h2} \tan\delta \\ \tau_{s2} = \sigma_{n2} \tan\delta \\ dw_2 = \gamma(ef + gh)dy/2 \end{cases} \tag{26}$$

The horizontal force balance of the differential element

reveals that:

$$\sigma_{h2}dy + \tau_s dy \cot\alpha - \sigma_{n2}dy = 0 \quad (27)$$

and the vertical force balance reveals that:

$$\sigma_{v2}ef + dw - (\sigma_{v2} + \mathrm{d}\sigma_{v2})gh - \tau_s dy - \tau_w dy - \sigma_{n2}dy\cot\alpha = 0 \quad (28)$$

Moreover, substituting Eqns. (5), (25) and (26) into Eq. (28), and neglecting the second-order differential parts, yields Eq. (29):

$$\frac{\mathrm{d}\sigma_{v2}}{\mathrm{d}y} = \gamma + \frac{1}{ab}[\sigma_{v2}\tan(\theta-\varphi) - \tau_s - \tau_w - \sigma_{n2}\tan(\theta-\varphi)] \quad (29)$$

Thus, the simultaneous equation of Eqns. (27) and (29) yields the average vertical stress of the differential element

$$\frac{\mathrm{d}\sigma_{v2}}{\mathrm{d}y} = \gamma + \lambda\sigma_{v2} \quad (30)$$

where

$$\lambda = \frac{\tan(\theta-\varphi) - K_{awn2}(\tan\delta + \tan\theta)}{ab} \quad (31)$$

The lateral earth pressure σ_{h2} in Zone 2 is then given by Eq. (39):

$$\sigma_{h2} = K_{awn2} \times \sigma_{v2} \quad (32)$$

Further, the resultant active earth pressure E_{a2} in Zone 2 is given by Eq. (40):

$$E_{a2} = \frac{\int_{A_3}^{A_2}\sigma_{h2}dy}{\cos\delta} \quad (33)$$

where

$$A_2 = r_j\sin\theta_j = r_0\exp[(\theta_j-\theta)\tan\varphi]\sin\theta_j$$

$$A_3 = r_h\sin\theta_h$$

Finally, the resultant lateral active earth pressure E_a of the retaining wall can be expressed as Eq. (34):

$$E_a = E_{a1} + E_{a2} = \frac{\int_{A_2}^{A_1}\sigma_{h1}dy + \int_{A_3}^{A_2}\sigma_{h2}dy}{\cos\delta} \quad (34)$$

where

$$A_1 = r_0\sin\theta_0$$

$$A_2 = r_j\sin\theta_j = r_0\exp\left[(\theta_j-\theta_0)\tan\varphi\right]\sin\theta_j$$

$$A_3 = r_h\sin\theta_h = r_0\exp\left[(\theta_h-\theta_0)\tan\varphi\right]\sin\theta_h$$

C. Solving the Equation Using the Difference Method

For the partition calculation, Eq. (41) contains the parameter θ, the value of which changes with the change in filling depth *h*. The solution can be facilitated by using the difference method in the MATLAB software. With reference to Figs 8 and 9, the vertical stresses in layer *i* of Zone 1 and layer *ii* of Zone 2 can be expressed as follows:

$$\begin{cases}\sigma_{v1}^{i} = \sigma_{v1}^{i-1} + \mathrm{d}\sigma_{v1}^{i} \\ \sigma_{v2}^{ii} = \sigma_{v2}^{ii-1} + \mathrm{d}\sigma_{v2}^{ii}\end{cases} \quad (35)$$

where σ_{v1}^{i} and σ_{v2}^{ii} are the vertical stresses in layer *i* of Zone 1 and layer ii of Zone 2, σ_{v1}^{i-1} and σ_{v2}^{ii-1} are the vertical stresses in layer *i*-1 of Zone 1 and layer *ii*–1 of Zone 2, and $\mathrm{d}\sigma_{v1}^{i}$ and $\mathrm{d}\sigma_{v2}^{ii}$ are the incremental vertical stresses in layer *i* of Zone 1 and layer ii of Zone 2. Meanwhile, the lateral stresses in layers *i* and *ii* of Zones 1 and 2 can be expressed as follows:

$$\begin{cases}\sigma_{h1}^{i} = K_{awn1}\sigma_{v1}^{i} \\ \sigma_{h2}^{ii} = K_{awn2}\sigma_{v2}^{ii}\end{cases} \quad (36)$$

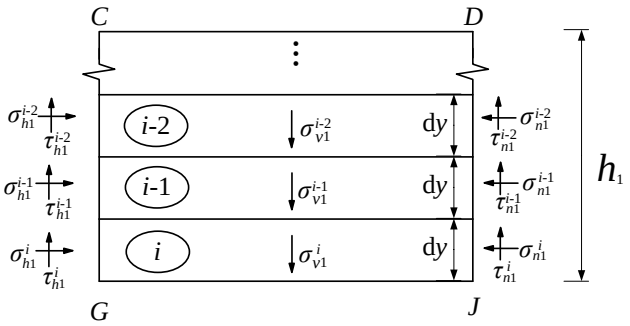

Fig. 8. The finite difference method for the layering in Zone 1.

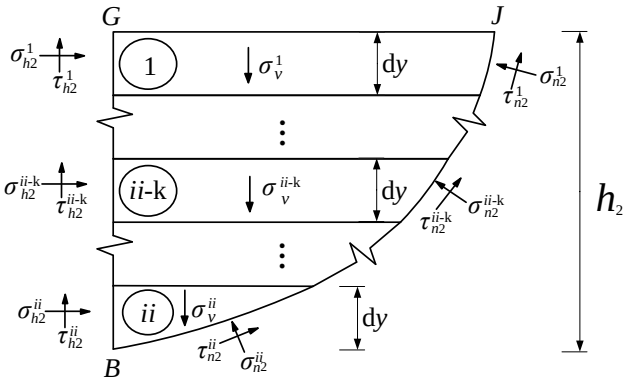

Fig. 9. The finite difference method for the layering in Zone 2.

The overturning moment *M* of the active earth pressure can then be obtained by integration:

$$M = \sum_{i=1}^{i}\sigma_{h1}^{i}(H-y_1)\mathrm{d}y + \sum_{ii=1}^{ii}\sigma_{h2}^{ii}(H-y_2)\mathrm{d}y \quad (37)$$

The Eq. (34) can be transformed into Eq. (38):

$$E_a = \sum_{i=1}^{i}\frac{\sigma_{h1}^{i}\mathrm{d}y}{\cos\delta} + \sum_{ii=1}^{ii}\frac{\sigma_{h2}^{ii}\mathrm{d}y}{\cos\delta} \quad (38)$$

and the height h_t of its application point on the wall can be obtained from Eq. (39):

$$h_t = \frac{M}{E_a} \quad (39)$$

V. Validation of the Proposed Method

A. Comparison with the Model Test by Take and Valsangkar

Centrifuge model tests at an acceleration of 35.7g were performed by Take and Valsangkar for the backfill confined behind a retaining wall, wherein a model retaining wall of height 140 mm was equivalent to an actual retaining wall of height 5 m after centrifugal enlargement [22]. For the test conditions, the unit weight of the soil was taken as γ=15.87 kN/m^3, the critical internal friction angle of the soil was 29°, and the critical oil–wall interface friction angle was 23°. For validating the model, the narrow backfill widths were *L*=38and 15 mm, corresponding to the narrow backfill widths of X_1 =1.36 and 0.53 m, respectively, in the actual project. In Fig. 10, the model is verified by comparison with the working conditions where the friction angles between the wall and soil

δ and between the soil and the rock surface φ are equal, using φ = 29°and δ = 23°as the test parameters in the critical state.

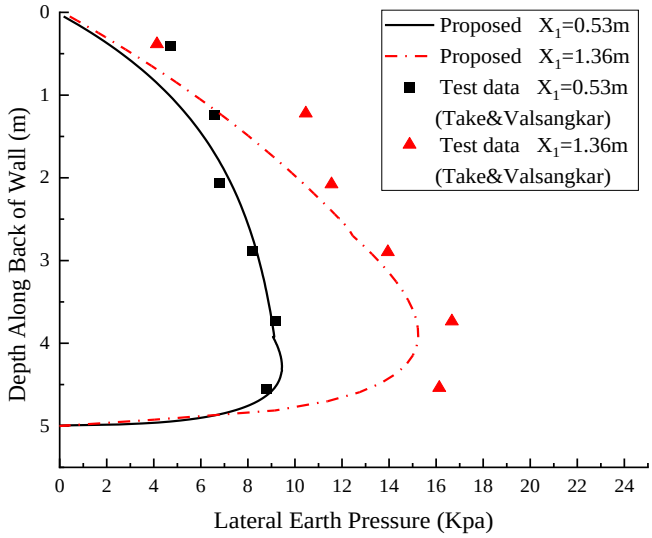

Fig. 10. Comparison of the present theoretical solution with the experimental values of *Take* and *Valsangkar*.

B. Comparison with the Model Test by Yang

Yang [23] experimentally tested a model for the active earth pressure of narrow backfill wherein the dry density of the cohesionless filler was modelled as ρ = 1.488 g/cm^3, the internal friction angle of the soil was φ = 32.75°, the porosity ratio was e = 0.679. The soil–wall interface friction angle δ was not provided, and is assumed to be $\delta = 2\varphi/3$. There was no load on the surface of the fill. In the proposed model, the fill height behind the retaining wall was 1.3 m, and the narrow backfill widths were 0.36 and 0.16 m, respectively. This model is verified by comparing with experimental results in Fig. 11. Here, the nonlinear active earth-pressure curves got with the model are in generally excellent consistency with Yang's experimental values. However, the position where the maximum active earth pressure appears at a backfill width of 0.16 m is slightly lower in the model than in the experimental result.

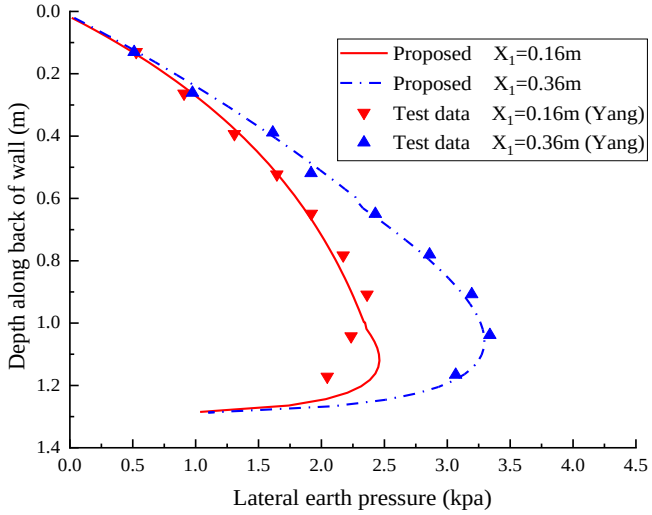

Fig. 11. Comparison between the proposed model and the experimental distributions of the lateral active earth-pressure force along the depth according to Yang.

VI. Parametric Analysis

As the impact of the soil–wall interface friction angle δ and backfill aspect ratio n on the distribution of earth pressure and its application point is this paper's main research content, the differences and relationships between the calculation theory proposed herein and the existing earth pressure theory are further discussed below, combined with parameter analysis. The parameters include the height of the retaining wall H =1.3 m, the unit weight of the soil γ =14.5824 kN/m^3, and the internal friction angle of the soil φ =32.75°.

A. The Effect of the Backfill Aspect Ratio

The depth along the back of the wall is plotted against the lateral earth pressure under different backfill aspect ratio n in Fig. 12. Here, the lateral earth pressure is seen to increase gradually as the backfill aspect ratio grows at a given depth, but the rate of increase in the lateral earth pressure gradually slows. Thus, the lateral earth pressure varies noticably with depth when $n < 0.5$, but is constant when $n \geq 0.5$. Therefore, n= 0.5 is the threshold value for distinguishing between finite and semi-infinite soils.

The impact of the different backfill aspect ratio n on the dimensionless height of the point of applying the resultant active earth pressure is presented in Fig. 13. This demonstrates that when the ratio between the friction angle of the soil-wall interface and the internal friction angle of the soil δ/φ takes the same value, with the increase in the backfill aspect ratio, h_t/H gradually approaches the corner and is always greater than H/3. When the backfill aspect ratio takes the same value, the application height of the resultant active earth-pressure gradually moves away from the heel of the wall as δ increases.

The change in the resultant active earth pressure with n is presented in Fig. 14. The results reveal that, as n increases in the narrow backfill, the resultant active earth pressure shows an initial uniform increase and then gradually stabilizes.

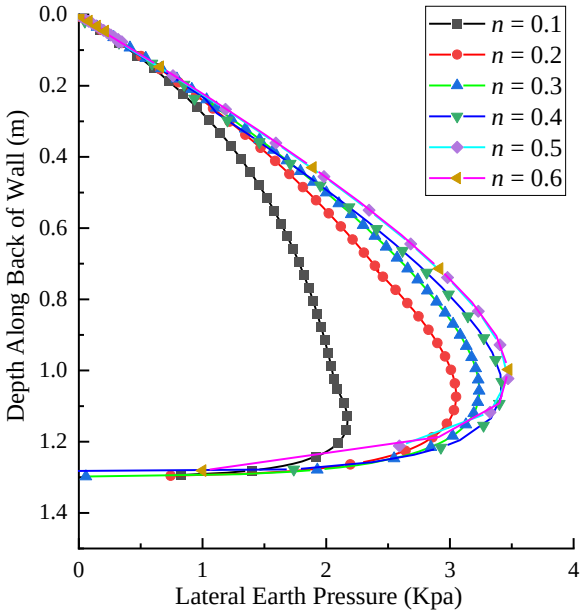

Fig. 12. The variation in lateral earth pressure with depth along the back of the wall under various backfill aspect ratios n= X_1/H.

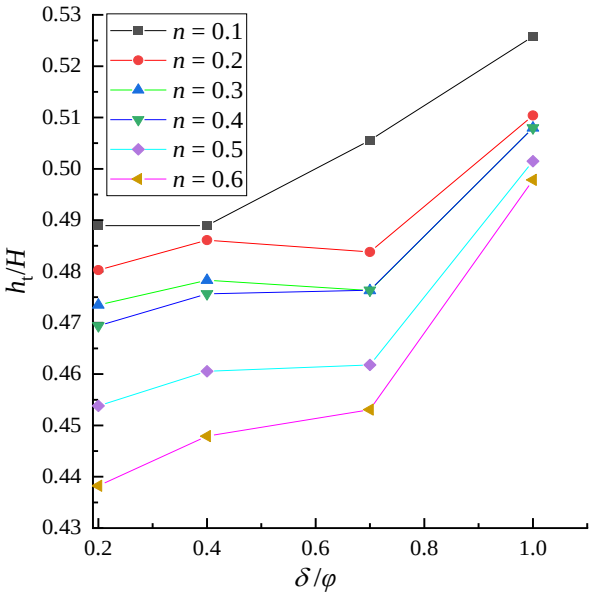

Fig. 13. The influence of backfill aspect ratio (n) on the dimensionless height (h_t/H) of the resultant active earth-pressure application point.

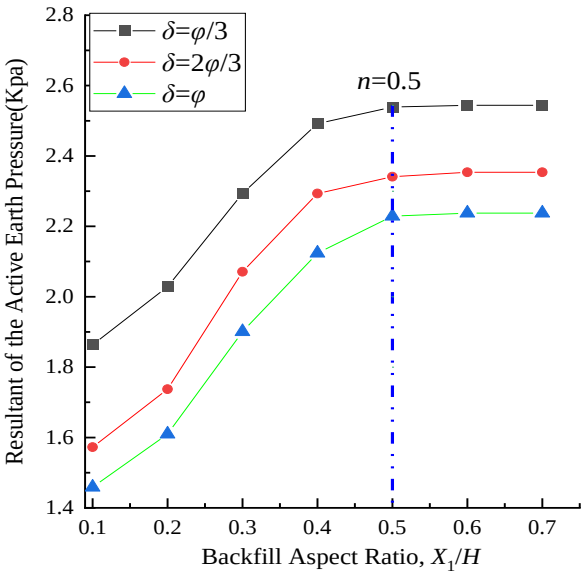

Fig. 14. The effect of backfill aspect ratio (n) on the resultant active earth pressure.

B. The Effect of the Soil—Wall Interface Friction Angle

In this section, the impact of the soil–wall interface friction angle δ on the allocation and height of usage h_t of the active earth pressure is investigated by setting φ = 40° and leaving the unit weight γ of the soil and the height (H) of the retaining wall unchanged. The results in Fig. 15 reveal that, when $\delta = \varphi/4$, the active earth pressure behind the wall is approximately triangular in allocation as the soil–wall interface friction angle grows, however, the earth pressure gradually shifts to a curvilinear distribution. Besides, the earth-pressure distribution shows little variation near the top of the wall, but gradually decreases near the bottom, while the point of maximum earth pressure rises, thereby resulting in a slight increase in the location of the resultant earth-pressure point.

Further, the results in Fig. 16 indicate that the ratio h_t/H gradually increases as the soil–wall interface friction angle δ is increased, and is always greater than $H/3$. When $\delta = \varphi$, the point of applying the resultant force moves further away from the heel of the wall as δ increases.

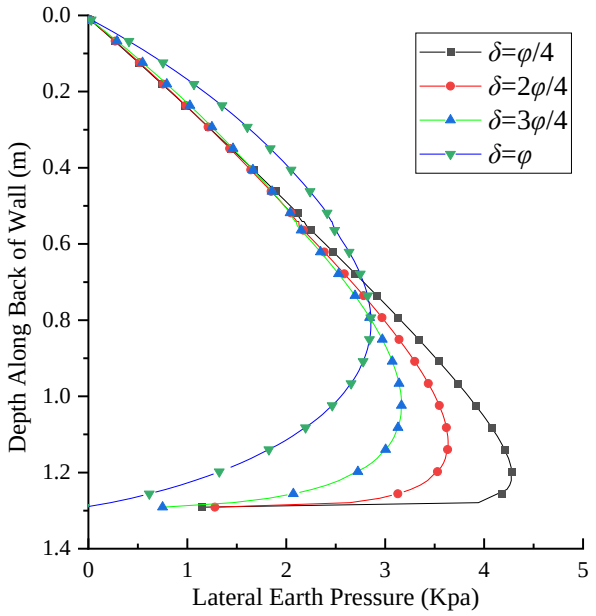

Fig. 15. The effect of the soil–wall friction angle on the lateral earth pressure along the depth.

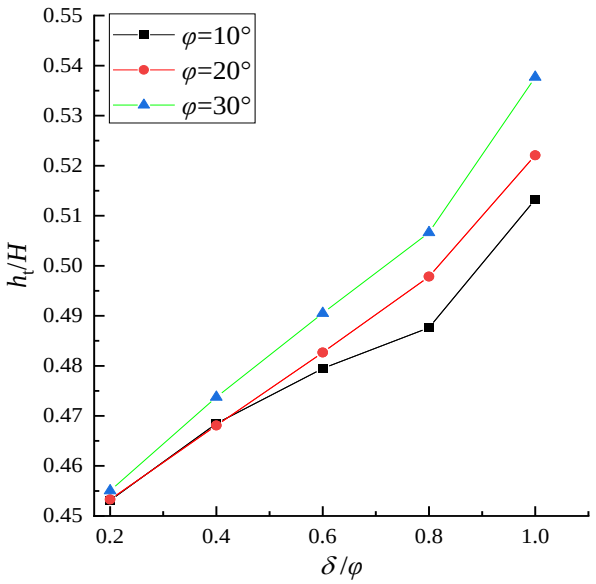

Fig. 16. The effect of various δ/φ ratios upon the application height of the resultant active earth-pressure.

VII. Conclusions

The friction between soil and a retaining wall inevitably deflects the point of application of the principal stress, thereby leading to the soil arch effect. Herein, the horizontal differential factor approach was adopted to research the failure mode of the curved–straight sliding crack surface with narrow backfill behind a wall. Moreover, based on the limiting equilibrium theory, an analytical method was established to calculate the active earth pressure of cohesionless soil under the translational mode of the retaining wall, and was used to reasonably explain the nonlinear allocation of the active earth pressure. The partition calculation of limited soil was used to make the model calculation more reasonable. Besides, the equations for the resultant active earth pressure and its height of application at the wall were obtained using the difference method. The earth pressure allocation was compared with the results of previous experimental tests and narrow backfill research. On basis of the parametric analysis, the conclusions were reached as

below:

1) The equations derived herein are in good agreement with the previous experimental results, thereby verifying the reasonableness of the proposed theory.

2) At various backfill aspect ratios *n*, the active earth pressure of the narrow backfill is nonlinearly distributed along the height of the wall, initially increasing steadily with depth in the soil, and then decreasing steadily near the bottom of the wall. When $n < 0.5$, the active earth pressure grows with the growth in *n*. When $n \geqslant 0.5$, the difference in the active soil pressure at the same depth is very small. Thus, $n = 0.5$ is the threshold value for distinguishing a limited backfill from infinite backfill.

3) The resultant active earth pressure of the retaining wall, and its relative height of application, are affected by the soil–wall interface friction angle and the backfill aspect ratio. As the backfill aspect ratio increases, the active earth pressure gradually increases, and its application point moves downward. As the soil–wall interface friction angle grows, the active earth pressure gradually decreases, and its usage point moves upward.

REFERENCES

[1] Coulomb C A, "Essai sur une application des regles de maximis et minimis a quelques problemes de statique relatifs a l'architecture. Mem. Acad. Roy. Sci. Pres. Sav., val. 7, pp. 343-382, 1776. 1973.

[2] Rankine, W. J. M.. I, "On the stability of loose earth," Philosophical transactions of the Royal Society of London, vol. 147, pp. 9-27, 1857.

[3] Fang, Y. S., & Ishibashi, I, "Static earth pressures with various wall movements," Journal of Geotechnical Engineering, vol. 112, no. 3, pp. 317-333, 1986.

[4] Terzaghi, K.. Theoretical soil mechanics, New York, 1943.

[5] Vermeer, P. A., Punlor, A., & Ruse, N, "Arching effects behind a soldier pile wall," Computers and geotechnics, vol. 28, no. 6-7, pp. 379-396, 2001.

[6] Handy, R. L, "The arch in soil arching." Journal of Geotechnical Engineering, vol. 111, no. 3, pp. 302-318, 1985.

[7] Kingsley Harrop-Williams, "Geostatic wall pressures," Journal of Geotechnical Engineering, vol. 115, no. 9, pp.1321-1325, 1989.

[8] K. H. Paik, & Rodrigo Salgado, "Estimation of active earth pressure against rigid retaining walls considering arching effects." Geotechnique, vol. 53, no. 7, pp. 643-653, 2003.

[9] Shubhra Goel, & Nihar Ranjan Patra, "Effect of Arching on Active Earth Pressure for Rigid Retaining Walls Considering Translation Mode," International Journal of Geomechanics, vol. 8, no. 2, pp.123-133, 2008.

[10] XU Ri-qing, XU Ye-bin, CHENG Kang, et, al, "Method to calculate active earth pressure considering soil arching effect under nonlimit state of clay," Chinese Journal of Geotechnical Engineering, vol. 42, no. 2, pp.362-371, 2020.

[11] Yu-Yong Jiao, You Zhang, & Fei Tan, "Estimation of Active Earth Pressure Against Rigid Retaining Walls Considering Soil Arching Effects and Intermediate Principal Stress," International Journal of Geomechanics, vol. 20, no. 11, 2020.

[12] Dalvi, R. S., & Pise, P. J, "Analysis of arching in soil-passive state," Indian Geotechnical Journal, vol. 42, no. 2, pp.106-112, 2012.

[13] Hong-wei, Y. I. N. G., JIANG, B., & Kang-he, X. I. E, "Distribution of active earth pressure against retaining walls considering arching effects," Chinese Journal of Geotechnical Engineering, vol. 29, no. 5, pp.717-722, 2007.

[14] Kumar, J, "Seismic passive earth pressure coefficients for sands," Canadian Geotechnical Journal, vol. 38, no. 4, pp.876-881, 2001.

[15] Subba Rao, K. S., & Choudhury, D, "Seismic passive earth pressures in soils," Journal of Geotechnical and Geoenvironmental Engineering, vol. 131, no. 1, pp. 131-135, 2005.

[16] Xie, Y., & Leshchinsky, B, "Active earth pressures from a log-spiral slip surface with arching effects." *Géotechnique Letters*, vol. *6, no.* 2, pp. 149-155, 2016.

[17] Fu-quan Chen, Cheng Lin, Luo-bin Lin, & Ming Huang, "Active earth pressure of narrow cohesive backfill on rigid retaining wall of rotation about the bottom", Soils and Foundations, vol. 61, no, 1, pp. 95-112, 2021.

[18] He, Z. M., Liu, Z. F., Liu, X. H., & Bian, H. B, "Improved method for determining active earth pressure considering arching effect and actual slip surface", Journal of Central South University, vol. 27, no. 7, pp. 2032-2042, 2020

[19] Zhu, et al. "Experimental Study on Passive Earth Pressure against Flexible Retaining Wall with Drum Deformation", Engineering Letters, vol. 29, no. 2, pp339-350, 2021

[20] WANG Kuihua, "Active Earth Pressure of Cohesive Soil Backfill on Retailing Wall with Curved Sliding Surface," JOURNAL OF SOUTHWEST JIAOTONG UNIVERSITY, vol. 46, no. 5, pp. 732-1–738, 2011

[21] Yang, M., & Tang, X. "Rigid retaining walls with narrow cohesionless backfills under various wall movement modes," International Journal of Geomechanics, vol. 17, no. 11, 2017

[22] Take, W. A., & Valsangkar, A. J, "Earth pressures on unyielding retaining walls of narrow backfill width," Canadian Geotechnical Journal, vol. 38, no. 6, pp. 1220-1230, 2001.

[23] YANG Minghui, "Soil Arch Effect Analysis and Earth Pressure Calculating Method for Finite Width Soil behind Retaining Wall," Journal of Hunan University (Natural Sciences), vol. 47, no. 3, pp. 19-27, 2017.